

# Chapter 2

## Metamaterials and Transformation Optics

Pi-Gang Luan

### 2.1 Introduction

Metamaterial is not a well-defined terminology. In fact, this terminology does not mean any specific material, but instead a new way of thinking. Usually this term means carefully engineered material structures composed of carefully designed inclusions that can exhibit unusual electromagnetic properties not inherent in the individual constituent components [1]. These properties include, for example, artificial magnetism [2], negative permeability [3], negative index of refraction [4], and hyperbolic dispersion [5, 6]. These properties lead to many fascinating phenomena such as negative refraction of light [7], sub-wavelength imaging [8], field enhancement [9], and evanescent-to-propagating wave mode conversion [5, 6], etc. Novel devices such as superlens [8–10], hyperlens [5, 6], invisibility cloak [11, 12], and plasmonic waveguide [13] based on these ideas have been designed, fabricated, and tested in the last decade.

The original purpose of initiating metamaterials research might be to construct artificial structures that can respond to electromagnetic waves intensively at any frequency we desire [2]. After this goal had been achieved, researchers then made a metallic periodic structure which behaves like an effective medium for EM waves having both negative permittivity [14] and negative permeability [3], and hence has a negative refractive index [4], realizing the ‘bending light to the wrong way’ phenomena predicted by V. G. Veselago more than 4 decades ago [7]. Furthermore, Pendry pointed out that a slab of negative refraction medium having appropriate negative permittivity and permeability not only cancels the phase accumulation of propagating waves but also amplifies the evanescent

---

P.-G. Luan (✉)

Wave Physics and Wave Engineering Lab/Department of Optics and Photonics,  
National Central University, 300 Chung-Da Rd, Chung-Li 32001, Taiwan  
e-mail: pgluan@dop.ncu.edu.tw

waves, thus can focus the light from a tiny source into a spot narrower than one wavelength, overcoming the diffraction limit [8, 9]. This ‘supelensing effect’ stems from the coupling between the source’s near fields (evanescent waves) and the surface plasmon-polariton (SPP) waves propagating along the slab boundaries. Pendry also argued that even if the relative permeability is nonnegative (close to 1), subwavelength imaging can still occur if the ‘quasi-static condition’ is satisfied [10].

After these concepts and predictions had been studied at the early stage, a tremendous amount of theoretical/numerical works have been done and a lot of experimental tests have been implemented. These developments finally helped to confirm the reality of negative refraction and subwavelength imaging phenomena [7–9] in the microwave frequency regimes. Recent studies further convinced that these notions still hold for optical waves [15]. However, some subtleties of metamaterials unnoticed before have been revealed [16–18]. For example, although a superlens can focus the light of a tiny source into a subwavelength spot; the image is located at the near field zone and cannot be further processed by conventional optical devices. The efforts to resolve this problem then led to the development of hyperlens [5, 6].

In addition to the above mentioned developments, there are many related research works, which include: negative refraction and subwavelength imaging of EM and acoustic waves by photonic crystal slab [19–28] and sonic crystal slab [29–32], negative refraction and subwavelength imaging of water waves [33, 34], acoustic metamaterials [35–37] and acoustic cloaking devices [38, 39], matter wave cloaks [40, 41], and plasmonic devices [42].

In this chapter we introduce some important topics in the metamaterials research and explain the essential physics related to them. However, we are not able to discuss all topics of this research area because it covers phenomena of too wide range and is evolving too fast. We provide very detailed discussions about wire array and split-ring resonator array structures in this chapter and derive the effective permittivity and permeability formulas for them, which might be helpful to a beginner.

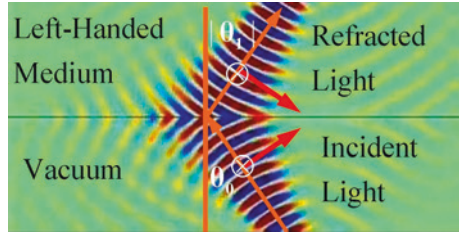
## 2.2 Negative Refraction, Flat Lens, and Perfect Lens

### A. Negative refraction and left handed media

Now we discuss the refraction behavior of a beam of light incident from an empty space to a left-handed medium (LHM) or double-negative medium (DNM). By DNM we mean the medium’s permittivity  $\varepsilon$  as well as its permeability  $\mu$  are negative. In Fig. 2.1, the medium above the interface (which is represented by a black horizontal line) is an LHM, and the medium below the interface is an empty space. The red arrows, white cross circles, and the orange colored arrows indicate the directions of the electric field  $\mathbf{E}$ , magnetic field  $\mathbf{H}$ , and Poynting vector  $\mathbf{S} = \mathbf{E} \times \mathbf{H}$ . For simplicity

**Fig. 2.1** Negative refraction.

Above the *black line* is the left-handed medium with  $\varepsilon < 0$  and  $\mu < 0$



we assume that  $\varepsilon \approx -\varepsilon_0$  and  $\mu \approx -\mu_0$  so that the impedance of the LHM is matched to that of the empty space, and the reflected waves can thus be neglected. According to Maxwell's equations, four boundary conditions (not all of them independent) should be satisfied at the interface, they are: the continuity of the normal components of the electric displacement field ( $D_n$ ) and magnetic induction ( $B_n$ ); and the continuity of the tangential components of the electric field ( $E_t$ ) and magnetic field ( $H_t$ ).

Set the orientations of the  $x$ ,  $y$ ,  $z$  axes to be along the rightward, upward, and outward directions of the page respectively, and choose the polarizations of the  $\mathbf{E}$  and  $\mathbf{H}$  fields as that shown in the empty space region of Fig. 2.1 (TM polarization), then the incident light has  $E_x^{inc} > 0$ ,  $D_y^{inc} = \varepsilon_0 E_y^{inc} > 0$ ,  $H_z^{inc} < 0$ , and  $S_x^{inc} < 0$ ,  $S_y^{inc} > 0$ . Using the boundary conditions for  $D_n$ ,  $B_n$ ,  $E_t$  and  $H_t$ , we conclude that the refracted light has  $E_x^{ref} = E_x^{inc} > 0$ ,  $D_y^{ref} = D_y^{inc} > 0$ , and  $H_z^{ref} = H_z^{inc} < 0$ . However, since the LHM has  $\varepsilon < 0$ , so  $D_y^{ref} = D_y^{inc} > 0$  implies  $E_y^{ref} = D_y^{ref} / \varepsilon < 0$ , and thus  $S_x^{ref} > 0$ ,  $S_y^{ref} > 0$ , as indicating in the LHM region of Fig. 2.1. Now, if we apply the Snell's law to the incident and refracted beams, a negative refractive index ( $n < 0$ ) must be assigned to the LHM because the refracted beam bends to the 'wrong way'. This argument explains why a DNM is a negative index medium (NIM), and similar argument can be applied to the TE polarization case. Furthermore, since the wave phase at the interface must be continuously connected, the wave front (the phase front) in the LHM region must propagate towards the interface, that is, the wave vector  $\mathbf{k}$  is antiparallel to the Poynting vector  $\mathbf{S}$ . Remember that in a usual medium with positive permittivity and positive permeability the  $\mathbf{E}$ ,  $\mathbf{H}$ , and  $\mathbf{k}$  triplet forms a right-handed coordinate system. However, the same triplet in a DNM forms a left-handed coordinate system. This explains why a DNM is called a LHM [7].

## B. LHM and metamaterials

Experimentally the LHM can be realized by fabricating artificial structures called metamaterials (see Fig. 2.2). In general metamaterials are not naturally existing materials or their simple mixtures or chemical products, instead, they are carefully designed structures such like thin metallic wires array, split-ring resonators (SRR) array, metal-dielectric multilayers [5, 6], fishnet structures [43], and helical metallic resonators array [44] etc. We will discuss in this chapter about how to realize negative permittivity and permeability by using wires and SRR arrays, and how to realize hyperbolic metamaterial [45] or indefinite medium [46] using metal-dielectric multilayers.



**Fig. 2.2** Two typical metamaterials consisting of metallic structures, both have negative refractive index in a certain frequency range. The metallic wires or rods provide the negative permittivity and the split-ring resonators provide the negative permeability. (Images: Physics Today, May 2000, 17; Science Vol. 292: 77, 2001)

In general metamaterials are dispersive media, which means the response of a metamaterial medium to the applied fields is frequency dependent. Usually they are also lossy or absorptive, which will degrade the NIM properties seriously. In fact, in the early stage of metamaterial research some researchers argued that due to the dispersive and absorptive properties, the negative refraction phenomenon in a metamaterial violates causality because it implies the possibility of superluminal propagation of signals. Besides, they even claimed that although the continuous waves of single frequency can deflect negatively, wave packet or beats always propagate positively [47]. However, after more careful analysis finally these arguments were found to be incorrect and thus these claims have been denied [48–50].

A simulation about beam propagation through a slab of LHM is shown in Fig. 2.3. The field strengths at 6 different times are revealed in the subplot (a) to (f), respectively. Comparing (b) with (c) or (e) with (f), one can find that the beam

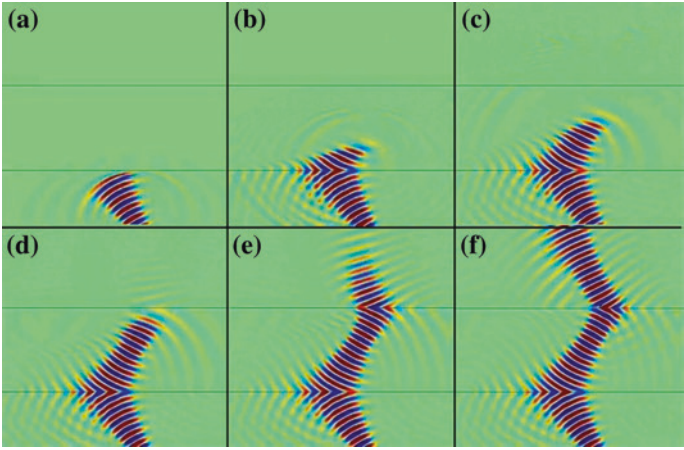


**Fig. 2.3** A Gaussian beam penetrates through an LHM slab that has a refractive index close to  $-1$  ( $n \approx -1$ ). **a–f** are the results of 6 successive times

propagating direction changes a little during the time interval between two successive instants. This fact implies that the LHM is a dispersive medium so the beam cannot keep its propagation direction unchanged.

### C. Electromagnetic energy density in metamaterials

There is another interesting issue concerning the LHM, that is, the electromagnetic energy density inside the metamaterials. We learned in the electrodynamics course that the electromagnetic energy density of time varying electromagnetic fields in a nondispersive medium is written as [51]

$$W = \frac{1}{2}\epsilon E^2 + \frac{1}{2}\mu H^2 \quad (2.1)$$

Here  $E^2$  and  $H^2$  are the square of the instantaneous  $\mathbf{E}$  and  $\mathbf{H}$  fields. Now if the permittivity and permeability become negative, what will be the expression of energy density? The above formula seems to imply the energy density becomes negative in such a medium, however, this is incorrect. In fact, for a dispersive medium without loss, Brillouin [52] and Landau [53] have already provided the following formula for the time average of the energy density (here  $\mathbf{E}$  and  $\mathbf{H}$  are the complex vector representation of the electric and magnetic field, respectively)

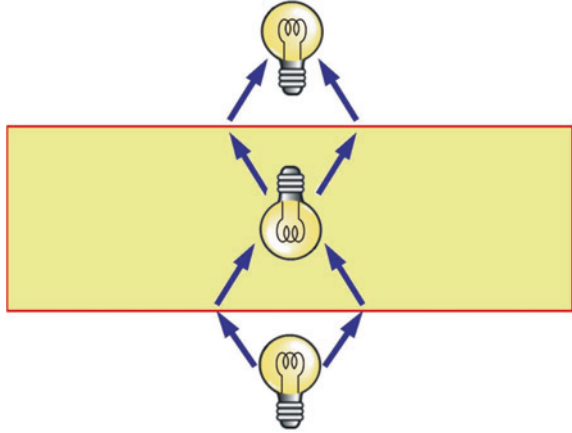
$$\langle W \rangle = \frac{1}{4}\epsilon_0 \frac{\partial(\omega\epsilon_r)}{\partial\omega} |\mathbf{E}|^2 + \frac{1}{4}\mu_0 \frac{\partial(\omega\mu_r)}{\partial\omega} |\mathbf{H}|^2 \quad (2.2)$$

which, if substituted the effective (relative) permittivity and permeability of the wire-SRR medium (referring to (2.12) and (2.26)), assuming the loss has been turned off, we get a positive result. For the cases with finite loss and the specific expressions for the electric and magnetic dipoles inside the medium are given, instantaneous energy density can also be derived, which is always positive and include three parts: the pure EM energy, the electric dipole energy, and the magnetic dipole energy [54]. In the latter two parts, the dipole energies may contain both the electric energy stored in the capacitors as well as magnetic energy stored in the inductances of the resonators that consist the medium.

### D. Flat lens and perfect lens

A very interesting consequence of negative refraction is that a slab of NIM is in fact a flat lens (see Fig. 2.4), which can focus the light emanating from a point source to two images, one inside and one outside of the slab, if the slab is thick enough [7]. This phenomenon can be understood in two ways, based on the languages of geometrical optics or wave optics. For simplicity we assume the refractive indices for the lens and the medium outside are  $-1$  and  $1$ , respectively. According to geometrical optics, light rays refract negatively across the interface between the positive and negative index materials. Since the flat lens has two interfaces, negative refraction happens twice, and the intersection points of different rays yield the two images. On the other hand, a focal point according to wave optics is a point having stationary wave phase. Since the regions inside and outside the slab lens have refractive indices  $-1$  and  $1$ , the two image points are just the two points having the same phase as that of

**Fig. 2.4** Flat lens made of a slab of LHM. It can focus the light from a point source



the source point. Light propagating outside the slab accumulates positive phase increment along the propagation direction, while negative phase difference is accumulated inside. The two images locate at the two points where the positive and negative phase accumulations cancel with each other completely.

Although the possibility of making a flat lens from a NIM had already been found by Veselago in 1967, people did not know before Pendry claimed that such a flat lens is a ‘perfect lens’, and it can be used to break the diffraction limit [8]. According to the traditional concepts of optics, light can be focused into a small spot, but the spot size (spot width) cannot be made much smaller than the wavelength. Such a restriction comes from the wave nature of light, and is sometimes called ‘diffraction limit’. In 2000, Pendry studied the EM properties of a slab made of a LHM having  $\epsilon_r = \mu_r = -1$ , and found that such a slab has  $n = -1$  and it not only can cancel the phases of propagating waves, but also can amplify the amplitudes of evanescent waves. Here  $\epsilon_r = \epsilon/\epsilon_0$  and  $\mu_r = \mu/\mu_0$  are the relative permittivity and relative permeability. This finding is astonishing because it implies that it is possible to achieve perfect imaging using such a flat lens. According to Pendry’s analysis, diffraction limit is mainly due to the fact that the information encoded in the evanescent waves of the light source is lost in the imaging process because of its exponential decay characteristic. However, the evanescent waves from the source can be amplified by the slab so they can contribute to the image. If the propagating and evanescent waves can be added properly at the image plane without losing any information, which Pendry claimed an  $n = \epsilon_r = \mu_r = -1$  slab in an empty space can do, then perfect imaging will happen. Notice that the choice of  $\epsilon_r = \mu_r$  is for the purpose of impedance matching so there would be no reflection and no information can be lost, whereas  $n = -1$  is for perfect phase cancellation of the propagating waves and perfect amplitude compensation of the evanescent waves.

The amplification of evanescent waves is relying on the mechanism of exciting the surface plasmon polaritons (SPPs). The condition  $\epsilon_r \approx \mu_r \approx -1$  in fact implies that the effective surface plasmon-polaritons (SPP) corresponding to both the electric



polarization resonance and the magnetization resonance have been excited efficiently by the evanescent fields from the source. Pendry further argued that even if the permeability is nonnegative, if  $\epsilon_r \approx -1$  is satisfied, subwavelength imaging can still occur if the slab thickness is much smaller than the wavelength (quasi-static condition). This kind of flat lens using only negative permittivity has already been fabricated and tested [10]. A flat lens having the ability of focusing light into a subwavelength spot no matter it uses perfect LHM or not is now called a ‘superlens’ [55].

The physics of surface plasmon can be understood as follows. In a metallic material of high conductivity such as silver or gold the conduction electrons or free electrons inside the material can move a long distance without being scattered. If we apply sinusoidally varying (harmonic) electromagnetic fields to the material, the free electrons would oscillate with the applied fields and move freely before being scattered by the phonons, dislocations, and defects, etc. However, if these electrons were moving close to the boundary of the metal, they would not be able to move outside far from the boundary and escape from the metal if they have not enough energy to overcome the ‘work function’. Note that inside the metal these electrons can move freely because the attractive forces due to the positive ions from all directions cancel with each other. However, once an electron moves to the boundary, the positive ions appear only on one side (the interior side) so a net ‘restoring force’ acts on it, forbidding the escaping of the electron from the metal. Note that the restoring forces acting on these electrons work just like many springs connected with them, which provide a resonance mechanism for forming SPPs. In the case of LHM slab the metal is replaced by a metamaterial having negative permittivity and negative permeability, and the true plasmon waves are replaced by the effective plasmon waves caused by the resonances of electric polarization and magnetization resonance of the medium.

No matter how great a perfect lens sounds like, any realization of such an ideal lens suffers from a number of restrictions due to the materials used or the structures being chosen. The first limitation comes from loss. A real material must absorb a part of the light energy, this effect limits the amplification of the evanescent waves, degrades the coherence of the light, and distorts the field distribution. All of them restrict the possibility of further reducing the spot size of the image. Another restriction is from the space period or lattice constant of the metamaterial. Such a characteristic length plays the role of cutoff length, and which implies that it is impossible to make an image narrower than the lattice constant [17]. In fact, in the early stage of perfect lens study, some researchers argued that the ideal perfect lens operating at the condition of  $\epsilon = \mu = -1$  is physically impossible because the energy stored in such a lens would be infinite, or some boundary conditions such as the continuity condition of wave phase would not be possible to satisfy [16]. This kind of controversies have never stopped but all of them are not directly related to the practical issues concerning applications [18]. Now we know that in practice the not-so-perfect negative refraction and subwavelength imaging are indeed realizable when properly designed metamaterials are used in making the lens (see Fig. 2.5).

Besides the above mentioned restrictions, people also found that the original designs of metamaterials which work well in the microwave frequency regime

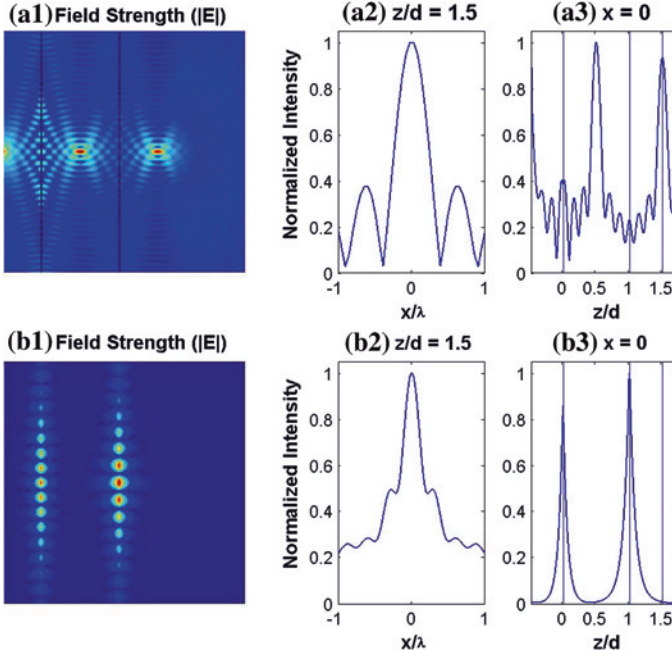


**Fig. 2.5** Field strengths ( $|E|$ ) and images made by a LHM flat lens. **a1–a3** show the case that the image size is within the diffraction limit, whereas **b1–b3** show the case of subwavelength imaging. The two boundaries of the lens are parallel to the  $x$  (vertical) axis, and the horizontal axis is the  $z$  axis. **a2** and **b2** are the (normalized) field strengths at the image plane. **a3** and **b3** are the (normalized) field strengths at the  $YZ$  plane

cannot do as well in the much higher frequency regime because the original circuit models for deriving the effective permittivity and permeability should be modified. For example, the resonance effect of SRRs becomes weaker at higher frequency due to electron's nonzero inertial mass, so that the desired negative permeability property becomes more difficult to achieve [56]. Thus for realizing negative refraction at optical or visible frequency regime some different structures must be used [57].

### 2.3 Photonic Crystals and Subwavelength Imaging

Negative refraction and subwavelength imaging can also be observed in photonic crystals (PhCs) made of nondispersive dielectric materials (see Fig. 2.6). The beam propagation direction inside a PhC is determined from the equal-frequency-surface (EFS) or constant frequency curve of the PhC [19–28]. The group velocity of the beam is along the direction normal to the constant frequency curve.

There are two kinds of slightly different mechanisms being used to achieve the unusual refraction/deflection and subwavelength imaging phenomena. The first



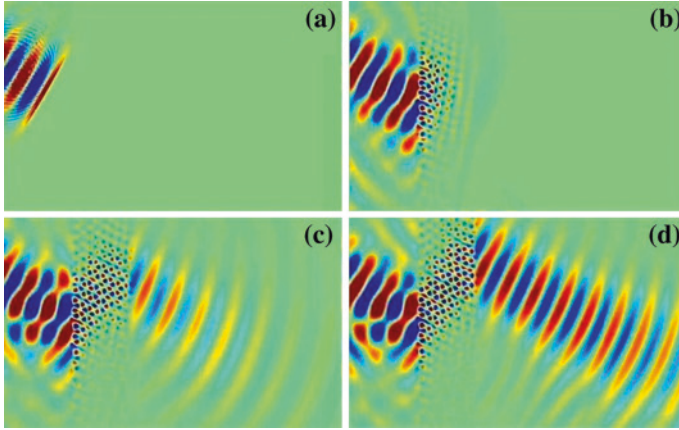
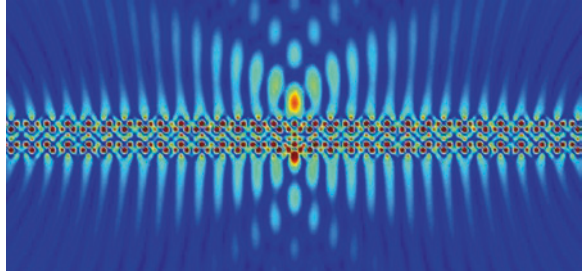


**Fig. 2.6** A Gaussian beam penetrates through an slab of photonic crystal which has a negative effective refractive index. **a–d** are the results of 4 successive times

**Fig. 2.7** Subwavelength imaging using photonic crystal slab



is the negative group index usually happening in the PhC with triangular lattice structures, the other is called all-angle negative refraction or canalization effect commonly encountered in the PhC with square lattice structures [20]. Deep sub-wavelength imaging is more easily to be achieved by using the canalization effect but the image always appears at the near field zone close to the PhC surface (see Fig. 2.7). However, negative refraction phenomenon is more easily to be observed using the negative group index mechanism [21]. Interested readers can learn the detailed knowledge from the textbook by Joannopoulos et al. [58].

## 2.4 Resonance, Constraints, and Metamaterials

The first experimental realization of DNM is a metallic structure consisted of periodically arranged metallic wires and split-ring resonators (SRRs) [3, 4]. In 1996, Pendry et al. [14] found that an array of thin wires behaves like an artificial

plasma, which yields a negative effective permittivity under the influence of an incident wave, if the frequency of the wave is appropriately chosen. This finding opened the doors of constructing these artificial media called ‘metamaterials’ using carefully designed metallic structures. In 1999, these researchers further showed theoretically that the periodically arranged Swiss roll structures or SRR array provide negative effective permeability in a range of frequency [2]. In the following two subsections we will give simple explanation about why a wire-array is an effective plasma medium, and then in the next subsection we will further argue why an SRR array can provide negative effective permeability in a certain range of frequency.

### A. Realization of negative permittivity

We first review briefly the concept of plasma medium. For simplicity we define plasma medium as the medium containing a lot number of charges that can move long distances without scattering. Many metals (for example, gold and silver) can be treated as plasma media at appropriate frequencies. The simplest model for describing the electromagnetic behaviors of plasma is the Drude model. According to this model, the free charges (electrons) are accelerated by the applied external (electric) field and move freely until being scattered by the defects, dislocations, and phonons etc. inside the medium (the metal). The scattering causes the relaxation of the kinetic energy of these charges, and the generation of heat. In Drude model, every free charge is assumed to be moving independently, and the energy relaxation process is described effectively by including a phenomenological damping force in the equation of motion.

For simplicity, we assume the applied electric field is along the  $x$  axis, and each charge is  $q$ . The equation of motion is written as

$$m \frac{dv}{dt} + bv = qE \quad (2.3)$$

Here  $v = \frac{dx}{dt}$  is the velocity of the charge,  $-bv$  is the damping force,  $x$  is the displacement of the charge. Under the condition of harmonic (single frequency) applied field, we adopt the complex representation (phasor representation) of the physical quantities and assume the time factor being  $e^{i\omega t}$ , that is,  $x = x_0 e^{i\omega t}$  and  $E = E_0 e^{i\omega t}$ , we can find the solution

$$x = -\frac{qE}{m} \left( \frac{1}{\omega^2 - i\Gamma\omega} \right) \quad (2.4)$$

where  $\Gamma = b/m$  is a dissipation coefficient, corresponding to the damping force.

We now derive the relative permittivity  $\varepsilon(\omega)$ . The constitutive relation between the  $E$  and  $D$  fields is

$$D = \varepsilon_0 E + P = \varepsilon_0 \varepsilon(\omega) E \quad (2.5)$$

where  $P$  is the polarization field. For the sake of simplicity, here we have dropped the subscript  $r$  of the relative permittivity notation. Assume that the concentration

of the free charge is  $N$ , we get  $P = Nqx$ , here  $qx$  is the electric dipole of a single charge. From (2.4) and (2.5) we find

$$\varepsilon(\omega) = 1 + \frac{P}{\varepsilon_0 E} = 1 - \frac{\omega_p^2}{\omega(\omega - i\Gamma)} \quad (2.6)$$

where  $\omega_p$  is the plasma frequency, defined by

$$\omega_p = \sqrt{\frac{Nq^2}{m\varepsilon_0}}. \quad (2.7)$$

When  $\Gamma$  is negligible, we have  $\varepsilon(\omega) < 0$  if  $\omega < \omega_p$ . That is, for electromagnetic wave with  $\omega < \omega_p$ , the plasma medium has negative permittivity.

Now we turn to the discussion of wires array medium. For simplicity we consider only the two dimensional case. We assume the wires are located at the lattice points of a square lattice, and the applied field is parallel to the wires (along the direction of the  $z$  axis). Denote the lattice constant as  $a$ , the radius of the wires as  $r$ , and assume the charge concentration inside the wires is  $N$ . The array is in fact a metallic photonic crystal (MPC), thus the electromagnetic behaviors of this structure can be understood from the results of its photonic band structure (PBS). However, in 1996, Pendry et al. found that if the wavelength of the applied field is much longer than the lattice constant, then an effective medium theory for this MPC can be constructed without referring to the PBS. Here we show how to derive the relative permittivity of this effective medium. Before we derive this result, first note the following differences between the ‘true plasma medium’ and the wire array structure: 1. The charges are confined inside the wires, and the current caused by the charge motion can only flow along the  $z$  direction, 2. The cross section area  $\pi r^2$  of each wire is much smaller than the unit cell area  $a^2$  of the lattice, thus the effective concentration  $N_{eff} = \pi r^2 N / a^2$  is also much smaller than the true concentration  $N$  inside the wires, 3. Every wire has a non-negligible self-inductance because there is an azimuthal directed magnetic field around the wire, and this magnetic field is not appearing in the original Drude model. Pendry argued in [14] that the vector potential of this magnetic field provides a modification to the charge’s canonical momentum, and if we treat the canonical momentum as a kinetic momentum without vector potential, then the effective mass of the electron should be redefined as a function of  $a$  and  $r$ . Here we provide an alternative derivation of Pendry’s result as follows.

Consider a segment of a wire, which has length  $l$ , self-inductance  $L$ , and resistance  $R$ . Apply the harmonic  $E$  field to the wire, then the potential drop along this segment is  $V = El$ . Suppose the current in the wire is  $I$ , then we have the circuit equation

$$L \frac{dI}{dt} + RI = El. \quad (2.8)$$

Simple observation indicates that the (2.8) can be cast into the same form as (2.3)

$$m_{eff} \frac{dv}{dt} + b_{eff} v = qE. \quad (2.9)$$

provided that we define the effective mass  $m_{eff}$  and damping coefficient  $b_{eff}$  as

$$m_{eff} = \frac{qLI}{lv}, \quad b_{eff} = \frac{qRI}{lv}. \quad (2.10)$$

The drift velocity  $v$  of the charges is related to the current  $I$  through  $I = \pi r^2 (Nqv)$ , so

$$m_{eff} = \frac{N\pi r^2 L}{l} q^2, \quad b_{eff} = \frac{N\pi r^2 R}{l} q^2. \quad (2.11)$$

From (2.9) we find the formula of relative permittivity

$$\varepsilon_{eff}(\omega) = 1 - \frac{\omega_p^2}{\omega(\omega - i\Gamma)} \quad (2.12)$$

where the plasma frequency  $\omega_p$  and dissipation coefficient  $\Gamma$  are given by

$$\omega_p = \sqrt{\frac{N_{eff} q^2}{m_{eff} \varepsilon_0}} = \frac{1}{a} \sqrt{\frac{l}{L \varepsilon_0}}, \quad \Gamma = \frac{R}{L}. \quad (2.13)$$

The permittivity formula in (2.12) is indeed the same form as that of the plasma media in (2.6). We can further calculate approximately the self-inductance  $L = \Phi/I$  of the wire and rewrite the effective mass  $m_{eff}$  and plasma frequency  $\omega_p$  using geometric parameters. To estimate the magnetic flux  $\Phi$  around a wire, we ignore the contribution from neighboring wires and that inside the wire, and calculate the magnetic flux through the rectangle defined by the conditions (using cylindrical coordinates):  $z = 0$  to  $z = l$  and  $R = r$  to  $R = a$

$$L = \frac{\Phi}{I} = \frac{\mu_0}{I} \int_r^a H l dR = \frac{\mu_0 l}{I} \int_r^a \frac{I}{2\pi R} dR = \frac{\mu_0 l}{2\pi} \ln\left(\frac{a}{r}\right). \quad (2.14)$$

According to (2.11), this leads to

$$m_{eff} = \frac{\mu_0 N r^2 q^2}{2} \ln\left(\frac{a}{r}\right), \quad \omega_p = \sqrt{\frac{2\pi c^2}{a^2 \ln\left(\frac{a}{r}\right)}}. \quad (2.15)$$

These results are the same as those obtained in [14].

In fact, from (2.8) and (2.9) the following energy relations can be derived by multiplying them with  $I$  and  $v$ , respectively

$$\frac{d}{dt} \left( \frac{LI^2}{2} \right) + RI^2 = IV, \quad \frac{d}{dt} \left( \frac{m_{eff} v^2}{2} \right) + bv^2 = qEv \quad (2.16)$$

Note that the magnetic energy  $LI^2/2$  is stored in the magnetic field around a wire, and its value is the same as  $N\pi r^2 l m_{\text{eff}} v^2/2$ , which is the effective kinetic energy of the charges inside the volume of a unit cell  $la^2$ :

$$N\pi r^2 l \frac{m_{\text{eff}} v^2}{2} = \frac{LI^2}{2} \quad (2.17)$$

This equality implies that in the effective theory of wire-array medium the magnetic energy around the wire is identified with the kinetic energy carried by the massive charged particles in the corresponding Drude model (see (2.9)). This identification transforms the wire array structure to the effective plasma medium described by the equations of motion in the Drude model (see (2.3) and (2.9)).

### B. Realization of negative permeability

We have shown in the previous subsection that the free moving charges inside the metal provide a means to realize the negative permittivity of the medium effectively. However, such a mechanism is not possible for realizing negative permeability because there has no magnetic monopole been found yet. One thus should use different method to make the effective permeability negative. From the constitutive relation

$$\mathbf{B} = \mu_0(\mathbf{H} + \mathbf{M}) = \mu_0\mu(\omega)\mathbf{H} \quad (2.18)$$

which relates the  $\mathbf{B}$  field (magnetic induction),  $\mathbf{H}$  field (magnetic field) and  $\mathbf{M}$  field (magnetization), one can imagine that if resonance effect can be used to make  $\mu_0\mathbf{M} > \mathbf{B}$ , then the directions of  $\mathbf{B}$  and  $\mathbf{H}$  become opposite to each other, and the desired  $\mu(\omega) < 0$  result can be realized. Since magnetization  $\mathbf{M}$  is defined as the magnetic dipole moment per unit volume, and a magnetic dipole is physically a current loop, thus negative permeability can be realized in principle by an array of resonant current loops. The array of split-ring resonators (SRR array) is the most studied structure for realizing the negative permeability experimentally [3, 4]. If a harmonic  $\mathbf{H}$  field perpendicular to the ring plane is applied to the SRR array, alternating current can be induced in each ring if the frequency is properly chosen. For each ring the split gaps of the ring stop the currents and help to accumulate the positive and negative charges on the two sides of each gap, thus they provide the capacitance  $C$ , whereas the currents circulating in the ring generate magnetic field and hence provide the inductance  $L$  [2]. Therefore, each SRR is an  $LC$  resonator having resonance frequency  $\omega_0 = \frac{1}{\sqrt{LC}}$ . When the frequency  $\omega$  of the applied  $\mathbf{H}$  field approaches the resonance frequency  $\omega_0$ , the resonance of currents occurs, and the condition  $\mu_0\mathbf{M} > \mathbf{B}$  can be satisfied. This leads to the negative effective permeability.

We now derive the effective relative permeability  $\mu(\omega)$ [2]. The details may refer to [59]. Consider the SRR structures shown in Fig. 2.8. A number of SRRs are piled up in the  $y$  direction to form an SRR stack, which can be viewed as a solenoid. These SRR stacks are periodically arranged in the  $xz$  plane at a square lattice of lattice constant  $a$ . The  $y$  spacing between two successive SRRs in one stack is  $l$ . This array structure can be viewed as solenoids array.

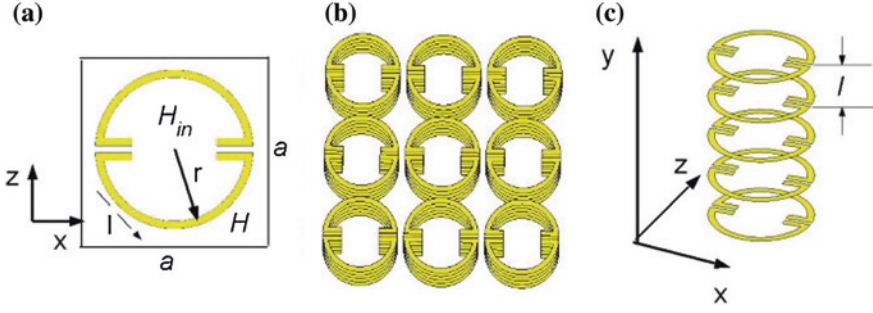


**Fig. 2.8** Array of split-ring resonators (SRRs). **a** A single SRR in a unit cell. **b** Array of SRR stacks. **c** An SRR stack formed by several SRRs arranged along the  $y$  direction

Now we apply an external harmonic  $H$  field of  $y$  direction, strength  $H_0$  to this SRR-stacks array. According to Faraday's Law, a current  $I$  is induced in each ring, thus a ring acquires a magnetic dipole moment  $m = I\pi r^2$ , here  $r$  is the radius of the ring. In a real structure, the number of rings in a stack is finite. Thus the field lines of the induced magnetic field which relate to the induced currents of the these rings 'spill out' from the terminals of the SRR stacks, contributing to the 'depolarization field'. If the wavelength of the incident  $H_0$  field is much longer than the lattice constant  $a$  and the  $y$ -spacing  $l$ , we can approximate the magnetic fields inside and outside the solenoid as two homogeneous fields  $H_{in}$  and  $H_{out}$ , respectively. According to Ampere's Law, the difference of them is given by

$$H_{in} - H_{out} = \frac{I}{l}. \quad (2.19)$$

Approximately assume that the depolarization flux is homogeneously distributed in the entire  $xz$  plane, and remember that the total flux caused by the induced currents is zero (because each of these magnetic field lines is closed), we get

$$FH_{in} + (1 - F)H_{out} = H_0, \quad (2.20)$$

where  $F = \pi r^2/a^2$  is the area filling fraction of a stack in a unit cell of the  $xz$  plane.

From (2.19) and (2.20) we find

$$H_{in} = H_0 + (1 - F)\frac{I}{l}, \quad H_{out} = H_0 - F\frac{I}{l}. \quad (2.21)$$

The magnetic induction  $B$  is defined as magnetic flux per unit area, therefore  $B = \mu_0 H_0$ . Besides, from (2.18) and the meaning of magnetization we have

$$H_0 = H + M, \quad M = \frac{m}{la^2} = F\frac{I}{l} \quad (2.22)$$

where  $M$  is the magnetization and  $la^2$  is the volume occupied by a ring. Comparing (2.21) with (2.22), one can make the identification:  $H = H_{out}$ . That is,



the magnetic field  $H$  in the effective medium is just the average magnetic field  $H_{out}$  in the ‘connected region’ outside the SRR stacks [2].

Now we calculate the magnetization  $M$  and derive the explicit expression of  $\mu(\omega)$ . The self-inductance  $L = \mu_0 F a^2 / l$  of an SRR in a chosen SRR-stack can be derived from the formula  $L = \Phi_s / I$ , where  $\Phi_s = \pi r^2 \mu_0 I / l$  is the flux through the SRR. In addition to  $L$ , the SRR also has a resistance  $R$ , a capacitance  $C$ , and a mutual inductance  $\mathcal{M} = -FL$  due to the depolarization fields spilled out from all the other SRR stacks in the array [2, 54, 59]. Under the influence of the  $H_0$  field, the current  $I$  in the SRR satisfies (note that the charges stored in the capacitance of the SRR is  $q = \int I dt$ )

$$(1 - F)L \frac{dI}{dt} + RI + \frac{q}{C} = -\frac{d}{dt} (F a^2 \mu_0 H_0), \quad (2.23)$$

Using the relation  $LI = \mu_0 M a^2$  and (2.22), (2.23) becomes

$$\frac{dM}{dt} + \gamma M + \omega_0^2 \int M dt = -F \frac{dH}{dt}, \quad (2.24)$$

where the dissipation coefficient  $\gamma$  and the resonance frequency  $\omega_0$  are defined as

$$\gamma = \frac{R}{L}, \quad \omega_0 = \frac{1}{\sqrt{LC}}. \quad (2.25)$$

Since the applied field is a harmonic field with frequency  $\omega$ , every dynamical quantity acquires the same time factor  $e^{i\omega t}$ . Thus from (2.18) and (2.24) we get the relative permeability:

$$\mu(\omega) = 1 - \frac{F \omega^2}{\omega^2 - \omega_0^2 - i\gamma \omega}. \quad (2.26)$$

This result is the relative permeability of the SRR medium. If  $\gamma$  is ignorable,  $\mu(\omega)$  becomes negative in the frequency range  $\omega_0 < \omega < \frac{\omega_0}{\sqrt{1-F}}$ . Note that in this derivation we did not use the specific expression of the capacitance  $C$  [2, 59].

## 2.5 Indefinite Media/Hyperbolic Metamaterials and Hyperlens

We have shown before that negative permittivity and negative permeability can be realized by using periodically arranged wires and SRRs, respectively. Simple observation tells us that these structures do not provide isotropic permittivity and permeability automatically if we do not arrange the orientations of these inclusions properly. For example, if in the 2D wire array all the wires are parallel to the  $z$  axis, than the standard effective plasma behavior will appear only when the electric field is also parallel to the  $z$  axis. In fact, if the wires are really thin enough, and we apply an  $E$  field perpendicular to them, then the structure

responds to the incident field just like the background medium (i.e., the empty space without these wires) does. Based on this consideration, it is not difficult to predict that the effective permittivity tensor for the array consisting of merely  $z$ -oriented wires has two different eigenvalues:  $\varepsilon_z = \varepsilon_{\parallel}$  and  $\varepsilon_x = \varepsilon_y = \varepsilon_{\perp}$ , so the  $z$ -oriented wires array is an uniaxial anisotropic medium. In this medium  $\varepsilon_{\perp}$  is in general positive but  $\varepsilon_{\parallel}$  takes negative value if the frequency is lower than the effective plasma frequency (see (2.12)). When the permittivity tensor of a uniaxial medium gives negative determinant, this medium is called ‘indefinite medium’ or ‘hyperbolic medium’. Metamaterials behave like hyperbolic media are called hyperbolic metamaterials. A multilayer structure made of one-dimensional photonic-crystal which contains one dielectric layer and one metal layer in one unit cell (one space period) also belongs to this category if the operating frequency is correctly chosen. In this chapter we will derive the effective permittivity of this structure and introduce the most important application of hyperbolic metamaterials: the hyperlens.

We have learned in the previous sections that a LHM has negative permittivity ( $\varepsilon < 0$ ) and negative permeability ( $\mu < 0$ ), leading to the negative refraction phenomena. Here we show that indefinite media or hyperbolic metamaterials with  $\varepsilon_{\perp} < 0$  can also bend the light beam to the ‘wrong way’ and gives an apparent negative refractive index referring to Snell’s law.

We refer to Fig. 2.1 again and consider TM polarized light, but now we replace the LHM region by an indefinite medium with  $\varepsilon_{\parallel} > 0$  and  $\varepsilon_{\perp} < 0$ . Here  $\varepsilon_{\parallel}$  and  $\varepsilon_{\perp}$  are the permittivity along the directions parallel and perpendicular to the interface, respectively. When this TM beam penetrates through the indefinite medium, the horizontal components of the  $\mathbf{E}$  and  $\mathbf{H}$  fields do not change. The vertical component of the  $\mathbf{D}$  field does not change too. However, since we have  $\varepsilon_{\perp} < 0$ , so the vertical component of the  $\mathbf{E}$  field changes sign just like that in the LHM case. We thus conclude that the Poynting vector  $\mathbf{S}$  (the light beam) bends negatively. Notice that in this argument the key point is the sign change of the vertical component of the  $\mathbf{E}$  field, and this happens only in the TM wave case ( $E_z = H_x = H_y = 0$ ) and does not apply to the TE wave case ( $H_z = E_x = E_y = 0$ ). Furthermore, we stress here that the phase propagation direction (i.e., the direction of the  $\mathbf{k}$  vector) in general is not along the direction of the beam direction (i.e., the direction of the Poynting vector  $\mathbf{S}$ ), so indefinite media are not LHM.

Now we derive the effective permittivity of the multilayer structure. Suppose the period of the structure is along the  $x$  direction, so the interface between the empty space and the structure is the  $yz$  plane. Consider a TM wave (P wave) incident from the empty space, and we choose the plane of incidence to be the  $xy$  plane, so the  $\mathbf{H}$  field is parallel to the  $z$  axis. Let the permittivities of the metal and dielectric layers to be  $\varepsilon_m$  and  $\varepsilon_d$ , and their thicknesses are  $a_m$  and  $a_d$ , respectively, so the period or lattice constant is  $a = a_m + a_d$ . To satisfy the continuity condition of the wave phase,  $k_y$  must be the same in each layer. We denote the  $k_x$  in the two layers as  $k_m$  and  $k_d$ , and use  $K$  to represent the Bloch wave number. When the wavelength of the incident wave is much longer than the lattice constant,  $\omega a/c$ ,

$k_m a_m$ ,  $k_d a_d$  and  $Ka$  take very small values. Under this condition, starting from the dispersion relation of one-dimensional photonic crystals [60]

$$\cos Ka = \cos k_m a_m \cos k_d a_d - \frac{1}{2} \left( \frac{k_m \varepsilon_d}{k_d \varepsilon_m} + \frac{k_d \varepsilon_m}{k_m \varepsilon_d} \right) \sin k_m a_m \sin k_d a_d \quad (2.27)$$

and expand the cosine and sine terms up to second order, we get the effective dispersion relation

$$\frac{K^2}{\langle \varepsilon \rangle} + \left\langle \frac{1}{\varepsilon} \right\rangle k_y^2 = \frac{\omega^2}{c^2} \quad (2.28)$$

where

$$\langle \varepsilon \rangle = \frac{a_m \varepsilon_m + a_d \varepsilon_d}{a}, \quad \left\langle \frac{1}{\varepsilon} \right\rangle = \frac{a_m / \varepsilon_m + a_d / \varepsilon_d}{a} \quad (2.29)$$

Now define  $k_{\parallel} = k_y$ ,  $k_{\perp} = K$ ,  $\varepsilon_{\parallel} = \langle \varepsilon \rangle$ , and  $1/\varepsilon_{\perp} = \langle 1/\varepsilon \rangle$ , we get the dispersion relation for this anisotropic effective medium

$$\frac{k_{\perp}^2}{\varepsilon_{\parallel}} + \frac{k_{\parallel}^2}{\varepsilon_{\perp}} = \frac{\omega^2}{c^2} \quad (2.30)$$

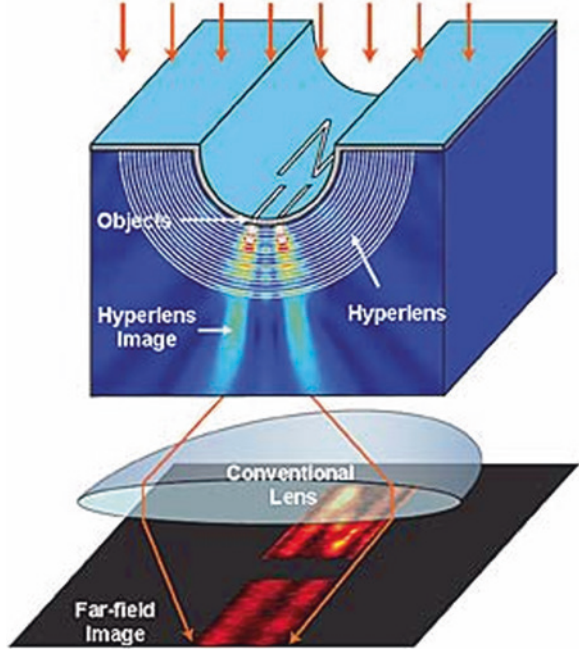
Choosing the filling fraction of the metal layer  $f = a_m/a$  and frequency (remember that  $\varepsilon_m = \varepsilon_m(\omega)$ ) properly, we can make  $\varepsilon_{\parallel} > 0$ ,  $\varepsilon_{\perp} = -|\varepsilon_{\perp}| < 0$ , and thus the dispersion relation in (2.30) becomes the hyperbolic form

$$\frac{k_{\perp}^2}{\varepsilon_{\parallel}} - \frac{k_{\parallel}^2}{|\varepsilon_{\perp}|} = \frac{\omega^2}{c^2} \quad (2.31)$$

This dispersion relation implies that both the propagating waves with  $|k_{\parallel}| \leq \omega/c$  and the evanescent waves with  $|k_{\parallel}| > \omega/c$  in an empty space can excite the propagating waves inside this indefinite medium, because for a finite  $\omega/c$ ,  $k_{\parallel}$  and  $k_{\perp}$  can take arbitrary large values.

We have explained in the previous sections that a slab of negative permittivity material such as a silver thin film behaves like a superlens, which means it can make a subwavelength image of a tiny light source. However, since the imaging mechanism of a slab lens relies on the evanescent waves, the image can appear only in the near field zone. Besides, the subwavelength image cannot be processed by conventional optical devices easily, thus a device that can make amplified image at the far field zone is desired. Hyperlens is indeed this kind of device to fulfill this requirement. A hyperlens is in fact a cylindrical device formed by curling up the multilayered structure of the dielectric-metal 1D photonic crystal (see Fig. 2.9). In a hyperlens, the  $\varepsilon_{\parallel}$ ,  $\varepsilon_{\perp}$ ,  $k_{\parallel}$  and  $k_{\perp}$  are replaced by  $\varepsilon_{\theta}$ ,  $\varepsilon_r$ ,  $k_{\theta}$ , and  $k_r$ , so we have  $\varepsilon_{\theta} > 0$ ,  $\varepsilon_r < 0$ , and the dispersion relation (2.31) becomes  $\frac{k_r^2}{\varepsilon_{\theta}} - \frac{k_{\theta}^2}{|\varepsilon_r|} = \frac{\omega^2}{c^2}$ .

**Fig. 2.9** Hyperlens and imaging through it. (Images courtesy of Zhang group, UC Berkeley)

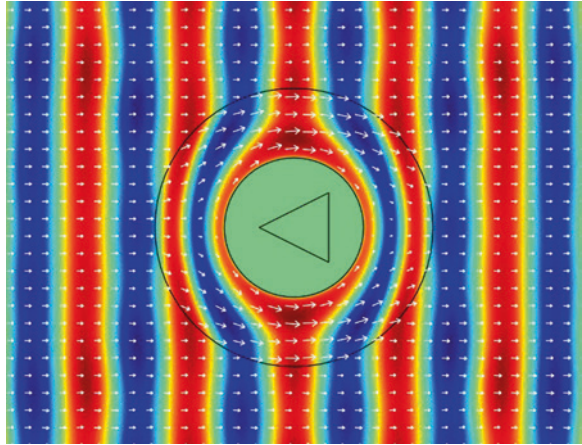


A small light source close to the inner surface of the hyperlens if emitting TM polarized light, then its evanescent waves can be coupled into the hyperlens and transformed into propagating waves inside. However, unlike in the flat lens case, the propagating modes inside this cylindrical structure are the products of Bessel function  $J_m(kr)$  and Neuman function  $N_m(kr)$  with the phase factor  $e^{im\theta}$ , where  $m$  is the order of the Bessel/Neuman function and  $k = \frac{\omega}{c}n$  is the wavenumber. The azimuthal component of the wave vector  $k_\theta = \frac{2\pi}{\lambda_\theta} = \frac{2\pi}{(2\pi r/m)} \sim m/r$  reduces as the radius increases. If the outer radius is large enough so that  $k_\theta(R) = m/R < \omega/c$ , then the image would be made of propagating waves and can appear in the far field zone [5, 6].

## 2.6 Invisibility Cloak and Transformation Optics

Now we introduce the concept of invisibility cloak and transformation optics [11, 12]. An invisibility cloak by definition is a shell made of carefully designed materials, and an object hidden inside as well as the shell itself would not be observed from outside. Light incident upon the cloak would not be scattered, and it can only propagate along the shell and goes back to the free space without penetrating through the cavity region enclosed by the shell. After leaving the cloak the light would propagate along the same direction as the original incident light, and no shadow will be formed (see Fig. 2.10). Since light does not penetrate into the

**Fig. 2.10** Electromagnetic waves propagating around an invisibility cloak. The white arrows indicate the direction and magnitude of the Poynting vectors. The triangle represents the object being hidden inside the cavity region



cavity region, the objects hidden inside would not have any electromagnetic interaction with the outside world.

In optics we know that the refractive index of media can influence the propagating direction of light. If the refractive index of a medium can be made a smooth function of position, then in principle a carefully arranged distribution of refractive index can guide light around a finite cavity region just like the desired invisibility cloak can do. However, this guiding would never be perfect and light scattering caused by internal reflection would make the cloak visible.

Is this fate unavoidable? To answer this question, remember that according to the electromagnetic theory of light, the refraction and reflection behaviors of light are in fact influenced by the relative permittivity  $\epsilon_r = \epsilon/\epsilon_0$  and relative permeability  $\mu_r = \mu/\mu_0$ , or equivalently by the refractive index  $n = \sqrt{\epsilon_r \mu_r}$  and relative impedance  $Z_r = \sqrt{\frac{\mu_r}{\epsilon_r}}$ . For usual optical media the magnetic response is weak so we can assume  $\mu_r = 1$  and get  $n = \sqrt{\epsilon_r} = \frac{1}{Z_r}$ . This reduces the independent material parameters from two to one and restricts the optical behaviors of the medium. In fact, the interface reflection of EM wave is caused by the impedance change, and not by the refractive index change. Thus if both the permittivity and permeability can be used, then it would be possible to guide light around an object without internal reflection.

To realize an invisibility cloak, John Pendry et al. proposed in 2006 a physically plausible scheme based on the idea of coordinate transformation [11]. In fact, it is known that the form of Maxwell's equations is invariant under a continuous and smooth coordinate transformation, although the expressions of the permittivity and permeability tensors after this transformation become anisotropic and inhomogeneous. That is, they are not simple constants or scalars but tensor densities [61]. After this early development, the same idea has been generalized to design other novel devices for controlling the light flows. Such kinds of researches are now categorized as 'transformation optics'(TO) [62, 63].

Now we explain why coordinate transformation can tell us how to design an invisibility cloak or other TO devices. We first choose a ‘target virtual space’ and define a coordinate transformation between the original space and this virtual one. The electromagnetic fields, light trajectories, and the media parameters (permittivity and permeability) would get their new expressions, directions, and values in this virtual space after the coordinate transformation. We then can treat the transformed media parameters as the true medium parameters in the original space and thus the transformed trajectories become the true trajectories of light in this original space if filled with the transformed medium. If the original space is empty, and we transform the space points inside a sphere of radius  $b$  to the shell region between  $a$  and  $b$  ( $a < b$ ) without changing the points outside the sphere, then a light ray originally goes straight through the sphere would become curved inside the shell and around the cavity  $r < a$ , and goes back to its original direction after leaving the shell. Thus the shell filled with the transformed medium is nothing but the desired invisibility cloak (see Fig. 2.11).

Now we derive the material parameters for the spherical cloak. First note that in the inner region  $r < b$ , the empty space has material parameters  $\varepsilon = \mu = 1$ . Here  $\varepsilon$  and  $\mu$  represent the relative permittivity and relative permeability, respectively. Now transform every point inside the sphere from  $(r, \theta, \varphi)$  to  $(r', \theta', \varphi')$  using the transformation:

$$r' = \left( \frac{b-a}{b} \right) r + a, \quad \theta' = \theta, \quad \varphi' = \varphi \quad (2.32)$$

A cavity of radius  $a$  is thus created, which corresponds the central point of the sphere. The shell region  $a < r' < b$  is from the whole interior region inside the sphere, except the central point. The new material parameters can be calculated according to the formula [64]

$$\varepsilon' = \frac{J \varepsilon J^T}{\det J}, \quad \mu' = \frac{J \mu J^T}{\det J} \quad (2.33)$$

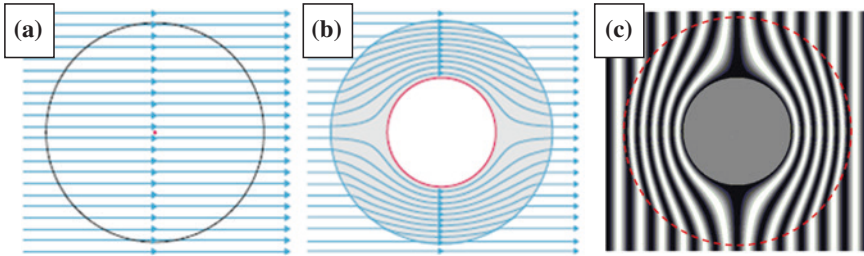


**Fig. 2.11** Invisibility cloak, the ray trajectories, and the phase of the electromagnetic waves. **a** A spherical region of empty space. **b** and **c** represent the effect of a invisibility cloak designed according to coordinate transformation. The curves with arrow heads are the ray trajectories, and the white and black colors in **c** represent the wave crests and wave troughs. (Images **a**, **b**: Science 313, 1399 (2006))



which yields

$$\varepsilon_{r'} = \mu_{r'} = \frac{b}{b-a} \left( \frac{r'-a}{r'} \right)^2 \quad (2.34)$$

$$\varepsilon_{\theta'} = \mu_{\theta'} = \frac{b}{b-a} = \varepsilon_{\varphi'} = \mu_{\varphi'} \quad (2.35)$$

These arbitrary material parameters in principle can be realized by using metamaterials. We have learned in the previous sections that in the long wavelength limit, periodic structures consisted of arrays of small electric and magnetic resonators such like wires and SRRs can work like a homogeneous medium having certain unusual permittivity and permeability, no matter it takes positive, negative, close to zero, or very large values. We can replace the smooth TO devices by an artificial structure consisted of a large amount of ‘metamaterial elements’ and approximate the material parameters as continuous functions if the changes of these parameters from an element to its neighboring element are really small enough.

Experimental realization of a 2D cylindrical cloak was first demonstrated in 2006 by David R. Smith’s group at Duke University [12]. They designed the 2D cloak for cloaking microwaves about 10 GHz, and their experiments confirmed that the cloak, though not perfect, can reduce the scattered wave dramatically. However, the parameters they used were not referring to the theoretical values directly from the coordinate transformation. The theoretical parameters were replaced by a set of reduced parameters, in which only the permeability tensor is varied along the radial direction, and the permittivity is a constant. A light ray propagating inside the shell region (now replaced by a ring region) would have the same trajectory as in the perfect cloak. However, reduced parameters do not satisfy the impedance matching conditions at the outer surface of the ring, so the scattered waves cannot be eliminated completely and thus the cloak is not perfect. In fact, designing transformation optics devices using metallic metamaterials with resonance property has some disadvantages. First, resonance implies the loss. As we have mentioned before, the energy loss of the electromagnetic wave causes the modification of the strength and phase of the wave, and they lead to the degradation of the device function such as the invisibility. Besides, resonance implies narrowband, so an invisibility cloak based on resonance mechanism can only work in a very narrow bandwidth, which is undesirable. Finally, it is difficult to fabricate metamaterials from nanostructures of resonant type, and as mentioned before, their resonance property are usually not good enough.

In order to avoid the above mentioned disadvantages, new designs of cloaking devices often use the idea of gradient index and they are built with common dielectric materials. One of them is the carpet cloak [65–67]. When covers this kind of cloak on an object lying on a table, the cloak can cancel the scattered light from the object completely, changing the table optically equivalent to a flat surface.

In addition to the various cloaking devices for controlling the electromagnetic waves, recently the similar ideas have been utilized and generalized for designing

devices for cloaking other kinds of waves. To build an acoustic cloak, we have to fabricate the acoustic metamaterials having the required effective mass density and bulk modulus or Lamé's constants. Such kind of cloaks have already been built and tested [38, 39]. People have also designed a cylindrical shaped water wave cloak for cloaking water waves by varying the water depth gradually along the radial direction around the cavity region [68]. This kind of cloaks may someday be used for protecting coastlines from tsunamis by making the land invisible to the incoming waves. Quantum wave cloaks or matter wave cloaks have also been considered, which guides the propagation of matter waves around a cloaked region by designing the effective mass and potential functions in the Schrodinger equation [40, 41]. A very interesting novel device called time cloak has also been proposed recently [69]. The fundamental concept of the previously mentioned cloaking devices is this: creating a hole in the space, and guide the waves around the hole by using properly designed artificial materials. The basic idea of time cloak is instead creating a gap in the time, and cheat the prob wave, making it unable to detect the event happening in the time gap. This description also explains why such a device is also called 'history editor' [70]. Reader may refer to the original papers and review articles for understanding these new developments [71].

## 2.7 Summary

In this chapter we have reviewed some topics in metamaterials research, which include: negative refraction, left-handed media, perfect lens or superlens and their relation with subwavelength imaging, the energy density problem, wire array and negative permittivity, SRR array and negative permeability, indefinite media or hyperbolic metamaterials and hyperlens, invisibility cloak and other transformation optics devices.

Metamaterials is in fact not materials but is a new way of thinking. With this new way of thinking people try every possible method to design structures for application and use them as materials. The most used mechanisms in designing metamaterials include resonance (SRR array), constraints for current flows (wire array), and high anisotropies (hyperbolic metamaterials). The effective media theories are useful but only accurate enough at the long wavelength limit. If the wavelength is not long enough we must treat metamaterials as what they really are, for example, photonic crystals consisting of periodic arranged metallic wires and split-rings. In that situation we must know the band structures or dispersion relations before we can make any predictions about the wave propagation properties inside these structures. Another very important issue is how to design broadband metamaterial devices which can work in a wide range of frequency. We are not able to discuss all the topics in this research area in only one section because it covers phenomena of too wide range and is evolving too fast. However, readers may find the materials provided in this chapter are essential and useful which can help them to pass through the main obstacles of understanding metamaterials.

## References

1. W.J. Padilla, D.N. Basov, D.R. Smith, *Mater. Today* **9**, 28 (2006)
2. J.B. Pendry, A.J. Holden, D.J. Robbins, W.J. Stewart, *IEEE Trans. Microw. Theory Tech.* **47**, 2075–2084 (1999)
3. D.R. Smith, W.J. Padilla, D.C. Vier, S.C. Nemat-Nasser, S. Schultz, *Phys. Rev. Lett.* **84**, 4184–4187 (2000)
4. R.A. Shelby, D.R. Smith, S. Schultz, *Science* **292**, 77–79 (2001)
5. Z. Jacob, L.V. Alekseyev, E. Narimanov, *Opt. Express* **14**, 8247 (2006)
6. Z. Liu, H. Lee, Y. Xiong, C. Sun, X. Zhang, *Science* **315**, 1686 (2007)
7. V.G. Veselago, *Sov. Phys. Usp.* **10**, 509 (1968)
8. J.B. Pendry, *Phys. Rev. Lett.* **85**, 3966–3969 (2000)
9. R. Merlin, *Appl. Phys. Lett.* **84**, 1290–1292 (2004)
10. N. Fang, H. Lee, C. Sun, X. Zhang, *Science* **308**, 534 (2005)
11. J.B. Pendry, D. Schurig, D.R. Smith, *Science* **312**, 1780 (2006)
12. D. Schurig, J.J. Mock, B.J. Justice, S.A. Cummer, J.B. Pendry, A.F. Starr, D.R. Smith, *Science* **314**, 977 (2006)
13. W.L. Barnes, A. Dereux, T.W. Ebbesen, *Nature* **424**, 824 (2003)
14. J.B. Pendry, A.J. Holden, W.J. Stewart, I. Youngs, *Phys. Rev. Lett.* **76**, 4773 (1996)
15. V.M. Shalaev, *Nat. Photonics* **1**, 41 (2007)
16. N. Garcia et al., *Phys. Rev. Lett.* **88**, 207403 (2002)
17. D. Maystre, S. Enoch, *J. Opt. Soc. Am. A*: **21**, 122 (2004)
18. P.G. Luan, H.D. Chien, C.C. Chen, C.S. Tang, *WSEAS Trans. Electron.* **1**, 236 (2004)
19. M. Notomi, *Phys. Rev. B* **62**, 10696 (2000)
20. C. Luo, S.G. Johnson, D.J. Joannopoulos, J.B. Pendry, *Phys. Rev. B* **65**, 201104 (2002)
21. S. Foteinopoulou, C.M. Soukoulis, *Phys. Rev. B* **67**, 235107 (2003)
22. E. Cubukcu, K. Aydin, E. Ozbay, S. Foteinopoulou, C.M. Soukoulis, *Nature* **423**, 604 (2003)
23. E. Cubukcu, K. Aydin, E. Ozbay, S. Foteinopoulou, C.M. Soukoulis, *Phys. Rev. Lett.* **91**, 207401 (2003)
24. S.S. Xiao, M. Qiu, Z.C. Ruan, S. He, *Appl. Phys. Lett.* **85**, 4269 (2004)
25. K. Guven, K. Aydin, K.B. Alici, C.M. Soukoulis, E. Ozbay, *Phys. Rev. B* **70**, 205125 (2004)
26. A. Martinez, H. Miguez, A. Griol, J. Mart, *Phys. Rev. B* **69**, 165119 (2004)
27. P. Vodo, P.V. Parimi, W.T. Lu, S. Sridhar, *Appl. Phys. Lett.* **86**, 201108 (2005)
28. P.-G. Luan, K.D. Chang, *J. Nanophotonics* **1**, 013518 (2007)
29. A. Sukhovich et al., *Phys. Rev. Lett.* **102**, 154301 (2009)
30. E. Di Gennaro et al., *Phys. Rev. B* **77**, 193104 (2008)
31. L.-S. Chen, C.-H. Kuo, Z. Ye, *Appl. Phys. Lett.* **85**, 1072 (2004)
32. P.-G. Luan, C.Y. Chiang, H.Y. Yeh, *J. Phys.: Condens. Matter* **23**, 035301 (2011)
33. X. Hu, Y. Shen, X. Liu, R. Fu, Z. Jian, *Phys. Rev. E* **69**, 030201 (2004)
34. X. Hu, C.T. Chan, *Phys. Rev. Lett.* **95**, 154501 (2005)
35. Z. Liu, X. Zhang, Y. Mao, Y.Y. Zhu, Z. Yang, C.T. Chan, P. Sheng, *Science* **289**, 1734 (2000)
36. J. Li, C.T. Chan, *Phys. Rev. E* **70**, 055602 (2004)
37. S. Zhang, L. Yin, N. Fang, *Phys. Rev. Lett.* **102**, 194301 (2009)
38. S. Zhang, C. Xia, N. Fang, *Phys. Rev. Lett.* **106**, 024301 (2011)
39. L. Zigoneanu, B.I. Popa, S.A. Cummer, *Nat. Mater.* **13**, 352 (2014)
40. S. Zhang, D.A. Genov, C. Sun, X. Zhang, *Phys. Rev. Lett.* **100**, 123002 (2008)
41. D.-H. Lin, P.G. Luan, *Phys. Rev. A* **79**, 051605 (2009)
42. *Nature Photonics* **6**, p. 707–p. 794 (2012)
43. J. Valentine, S. Zhang, T. Zentgraf, E. Ulin-Avila, D.A. Genov, G. Bartal, X. Zhang, *Nature* **455**, 376 (2008)
44. Z. Li, M. Mutlu, E. Ozbay, *J. Opt.* **15**, 023001 (2013)
45. A. Poddubny, I. Iorsh, P. Belov, Y. Kivshar, *Nat. Photonics* **7**, 948 (2013)
46. D.R. Smith, P. Kolinko, D. Schurig, *J. Opt. Soc. Am. B* **21**, 1032 (2004)

47. P.M. Valanju, R.M. Walser, A.P. Valanju, Phys. Rev. Lett. **88**, 187401 (2002)
48. J.B. Pendry, D.R. Smith, Phys. Rev. Lett. **90**, 029703 (2003)
49. D.R. Smith, D. Schurig and J. B. Pendry **81**, 2713 (2002)
50. S. Foteinopoulou, E.N. Economou, C.M. Soukoulis, Phys. Rev. Lett. **90**, 107402 (2003)
51. J.D. Jackson, Electrodynamics, 3rd edn. (Wiley, New York, 1998)
52. L. Brillouin, Wave propagation and group velocity (Academic Press, New York, 1960)
53. L.D. Landau, E.M. Lifshitz, *Electrodynamics of continuous media*, 2nd edn. (Pergamon Press, New York, 1984)
54. P.-G. Luan, Phys. Rev. E **80**, 046601 (2009)
55. X. Zhang, Z. Liu, Nat. Mater. **7**, 435–441 (2008)
56. J. Zhou, T. Koschny, M. Kafesaki, E.N. Economou, J.B. Pendry, C.M. Soukoulis, Phys. Rev. Lett. **95**, 223–902 (2005)
57. C.M. Soukoulis, M. Wegener, Nat. Photonics **5**, 523 (2011)
58. J.D. Joannopoulos, S.G. Johnson, J.N. Winn, R.D. Meade, *Photonic Crystals: Molding the Flow of Light*, 2nd Edn. (Princeton University Press, Princeton, 2008)
59. H. Chen, L. Ran, J. Huangfu, T.M. Grzegorzczuk, J.A. Kong, J. Appl. Phys. **100**, 024915 (2006)
60. P. Yeh, Optical waves in layered media (Wiley-Interscience, New York, 2nd edn, 2005)
61. Ulf Leonhardt, T.G. Philbin, New J. Phys. **8**, 247 (2006)
62. P. Sheng, Science **313**, 1399 (2006)
63. H. Chen, C.T. Chan, P. Sheng, Nat. Mater. **9**, 387 (2010)
64. S.G. Johnson, <http://www-math.mit.edu/~stevenj/18.369/coordinate-transform.pdf> (notes for the course 18.369 at MIT)
65. J. Li, J.B. Pendry, Phys. Rev. Lett. **101**, 203901 (2008)
66. T. Ergin, N. Stenger, P. Brenner, J.B. Pendry, M. Wegener, Science **328**, 337 (2010)
67. M. Gharghi, C. Gladden, T. Zentgraf, Y. Liu, X. Yin, J. Valentine, X. Zhang, Nano Lett. **11**, 2825 (2011)
68. M. Farhat, S. Enoch, S. Guenneau, A.B. Movchan, Phys. Rev. Lett. **101**, 134501 (2008)
69. J.M. Lukens, D.E. Leaird, A.M. Weiner, Nature **498**, 205 (2013)
70. M.W. McCall, A. Favaro, P. Kinsler, A. Boardman, J. Opt. **13**, 024003 (2011)
71. Y. Liu, X. Zhang, Nanoscale **4**, 5277 (2012)



<http://www.springer.com/978-94-017-9391-9>

The Current Trends of Optics and Photonics

Lee, C.-C. (Ed.)

2015, XXIII, 542 p. 357 illus., Hardcover

ISBN: 978-94-017-9391-9